Atomistic description of the electronic structure of $In_xGa_{1-x}As$ alloys and InAs/GaAs superlattices

Kwiseon Kim, P. R. C. Kent, and Alex Zunger
National Renewable Energy Laboratory, Golden, Colorado 80401

C. B. Geller
Bettis Atomic Power Laboratory, West Mifflin, Pennsylvania 15122
Received 12 March 2002; published 30 July 2002)

We show how an empirical pseudopotential approach, fitted to bulk and interfacial reference systems, provides a unified description of the electronic structure of random alloys bulk and epitaxial), superlattices, and related complex systems. We predict the composition and superlattice-period dependence of the band offsets and interband transitions of InAs/GaAs systems on InP and GaAs substrates.

DOI: 10.1103/PhysRevB.66.045208 PACS number s): 71.20.Nr, 71.15.−m

I. INTRODUCTION

InAs and GaAs are the building blocks of a diverse range of optoelectronic heterojunction systems, including i) short-period superlattices $(InAs)_n$

The various InAs/GaAs systems discussed above as well as other isovalent and isostructural semiconductor pairs) all

LDA calculations[54,55] predict a *large negative* $a_c < 0$ deformation potential for the CBM, and small deformation poten-

varied, plane waves are added or subtracted, potentially significantly increasing or decreasing the flexibility of the basis set. In order to minimize this effect, we find it beneficial to apply a weighting function to the individual plane waves

$$w_G = \frac{\cos\quad)+1}{2}, \tag{14}$$

$$= \tau\frac{E_G - E_{cut}}{1-\quad)E_{cut}}, \tag{15}$$

where E_G is the kinetic energy of the plane wave $|G + k|^2/2$. We find $=0.8$ provides an improved fit to cell-shape dependent properties such as hydrostatic and biaxial deformation potentials and alloy properties of strongly

A. Equilibrium atomic positions in superlattices

1. Continuum elasticity (CE) theory for strained superlattices

A film of a material grown epitaxially on a thick substrate will strain so that its atoms grow in registry with those of the substrate. Thus, its dimension $a_{\parallel}$, the lattice parameter of the layer parallel to the interface, becomes equal to that of the substrate a_s coherency condition), and $a_{\perp}$, the lattice parameter of the layer perpendicular to the interface, is determined by the strain tensor. Based on macroscopic continuum elasticity theory,[67–69]

$$a_{\perp}\ a_s,\hat{G})=a_{eq}-[2-3q\ \hat{G})]\ a_s-a_{eq}). \qquad 17)$$

Here, $\hat{G}$ is the direction of deformation and the epitaxial strain reduction factor is given by

$$q\ \hat{G})=1-\frac{B}{C_{11}+\quad \hat{G})\Delta}, \qquad 18)$$

where B is the bulk modulus, the C_{ij} are elastic constants of the embedded material, and

$$\Delta=C_{44}-\frac{1}{2}\ C_{11}-C_{12}) \qquad 19)$$

is the elastic anisotropy. is a purely geometric factor given by

$$\hat{G})= \quad , \ )=\sin^2\ 2\ )+\sin^4\ )\sin^2\ ), \qquad 20)$$

where are the spherical angles formed by $\hat{G}$. A general expression for $q(\hat{G})$ is given in Ref. 67. Explicit expressions for $q(\hat{G})$ along the principal directions 001), 011), 94 262.259 Tm (~)0.333s8t4303 and

$$C_{11}+2C_{12}=\sqrt{}$$

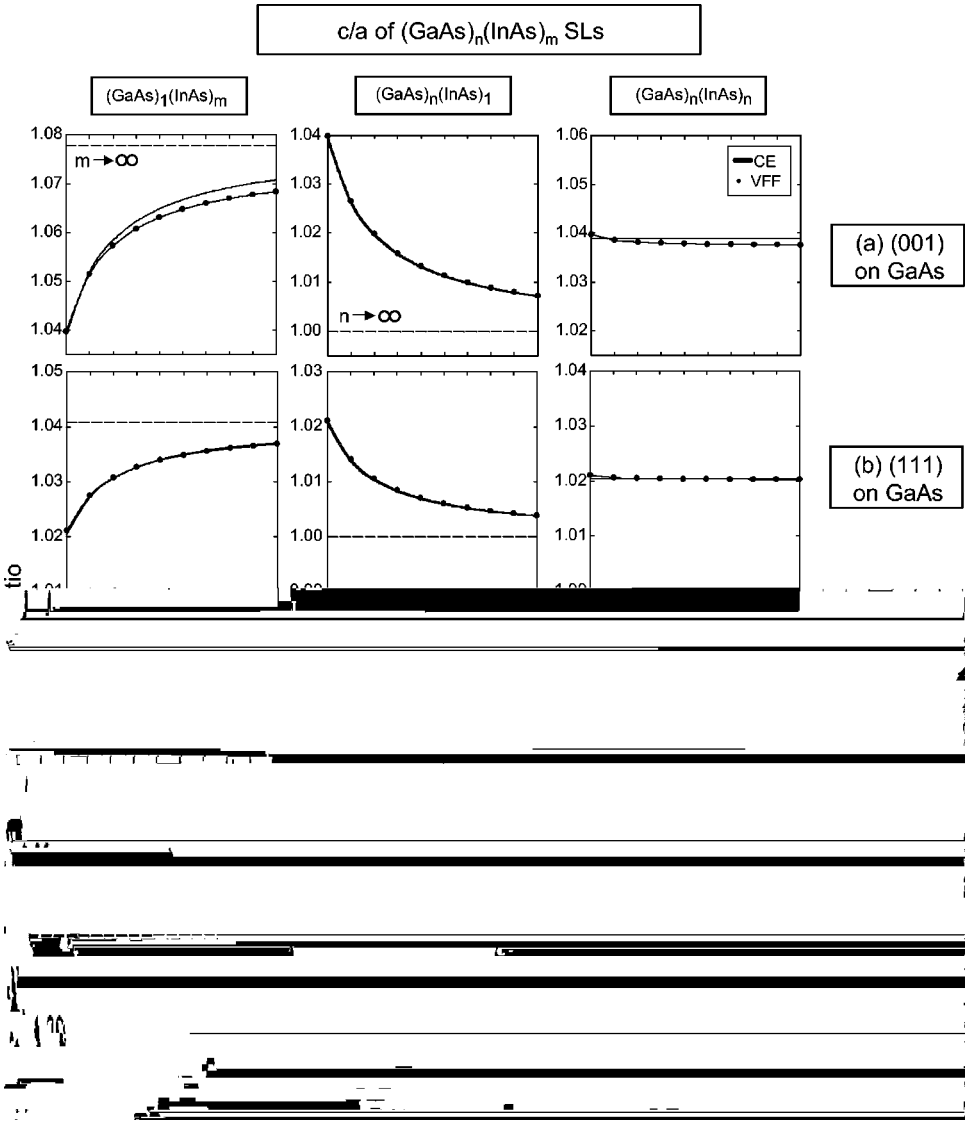

FIG. 2. c/a from continuum elasticity CE) [solid lines, Eq. 17)] and from VFF filled circles) for $(GaAs)_n(InAs)_m$ superlattices a) along 001) and b) 111) directions on GaAs, and c) along 001) and d) 111) directions on InP substrates. The asymptotic $n \rightarrow \infty$ values of c/a are shown as dashed lines.

$\rightarrow\infty$ are shown as dashed lines in Fig. 2. We see that continuum elasticity also works well for the c/a ratio.

4. VFF vs LDA for superlattices

As a simple test of our GVFF for alloy systems, we compared the relaxed atomic positions from GVFF with pseudopotential LDA results for a 100) $(GaAs)_1/(InAs)_1$ superlattice where the c/a ratio is fixed to 1, but we allow energy minimizing changes in the overall lattice constant (a_{eq}) and the atomic internal degrees of freedom (u_{eq}). We find

$$a_{eq}^{LDA} = 5.8612 \text{ Å},$$

$$u_{eq}^{LDA} = 0.2305,$$

while the GVFF results are

$$a_{eq}^{GVFF} = 5.8611 \text{ Å},$$

$$u_{eq}^{GVFF} = 0.2305.$$

A first-principles calculation by Bernard and Zunger[65] for $(InAs)_1(GaAs)_7$ 001) superlattice resulted in $\epsilon_\perp = 7.73\%$. Our GVFF gives 7.36%.

5. Atomic relaxation and interlayer spacing in InAs/GaAs superlattices

Figure 3 shows 001) and 111) interlayer distances in $(GaAs)_8/(InAs)_8$ superlattices. For an unrelaxed 001) superlattice, the internal coordinate z of the indium plane is 0.25 with respect to the c axis. The strain $\epsilon_\perp = (z - z_{equil})/z_{equil}$ is shown in Fig. 3. For an 111) superlattice, there are two internal coordinates, d_1 and d_2. The unrelaxed ideal) values are $d_1 = \sqrt{3}/4$ and $d_2 = \sqrt{3}/12$. d_1 is the distance between Ga In) and As atom layers where the bond is along 111) directions and d_2 is the distance between Ga In) and As atom layers where the bond is along $(11\bar{1})$, $(1\bar{1}1)$, or $(\bar{1}11)$ directions. The strains $\epsilon_1 = (d_1 - d_{1,equil})/d_{1,equil}$ and $\epsilon_2 = (d_2 - d_{2,equil})/d_{2,equil}$ are shown in Fig. 3.

We see that on a GaAs substrate, the atoms of the GaAs segment of the superlattice SL) are unrelaxed, whereas the strain in the InAs segment is positive. Most atoms have constant strain, except the atoms next to the interface. On the other hand, on an InP substrate, the GaAs segment is dilated ($\epsilon_\perp < 0$) and the InAs segment is compressed ($\epsilon_\perp > 0$), even though the lattice constant of the SL is almost matched to that of the substrate.

B. Equilibrium atomic positions in random alloys

The GVFF also is used to determine equilibrium atomic positions in random alloys. Here we create a supercell and randomly occupy cation sites with Ga and In atoms, according to the concentration $In_{1-x}Ga_xAs$. We then minimize the GVFF elastic energy by displacing atoms to their relaxed positions. We use a conjugate gradient algorithm using analytically calculated forces for both atomic positions and $a_\perp$. In a previous study[66] we reported the results for the closely related $In_{1-x}Ga_xP$ alloy, so we will not repeat the results for $In_{1-x}Ga_xAs$ here. In both cases we find a bimodal distribution of the nearest-neighbor anion-cation bond lengths, and a multimodal distribution of the cation-cation distances. Details are given in Ref. 66.

IV. STRAIN-MODIFIED BAND OFFSETS

Once we have determined the equilibrium atomic positions, and have a reliable screened pseudopotential, we can solve the Schrödinger equation, Eq. 3), in the plane-wave basis of Eq. 5). We first solve the simplest case, epitaxially deformed InAs and GaAs. Here, we imagine that GaAs is coherently strained on a substrate whose lattice constant a_s ranges from that of GaAs to that of InAs. The tetragonal deformation $a_\perp(a$

InAs/GaAs band offsets for various substrates such as GaAs, InP, and InAs. The calculated strained offsets on these substrates are given in Fig. 5 for two orientations, 001) and 111).

V. BAND-EDGE STATES IN RANDOM $In_xGa_{1-x}As$ ALLOYS

Figure 6 shows the band-edge states and the band gaps of a) relaxed ''bulk'') In_xGa_{1-x}

crossover[15] around 50% In, and a very shallow offset, sug-

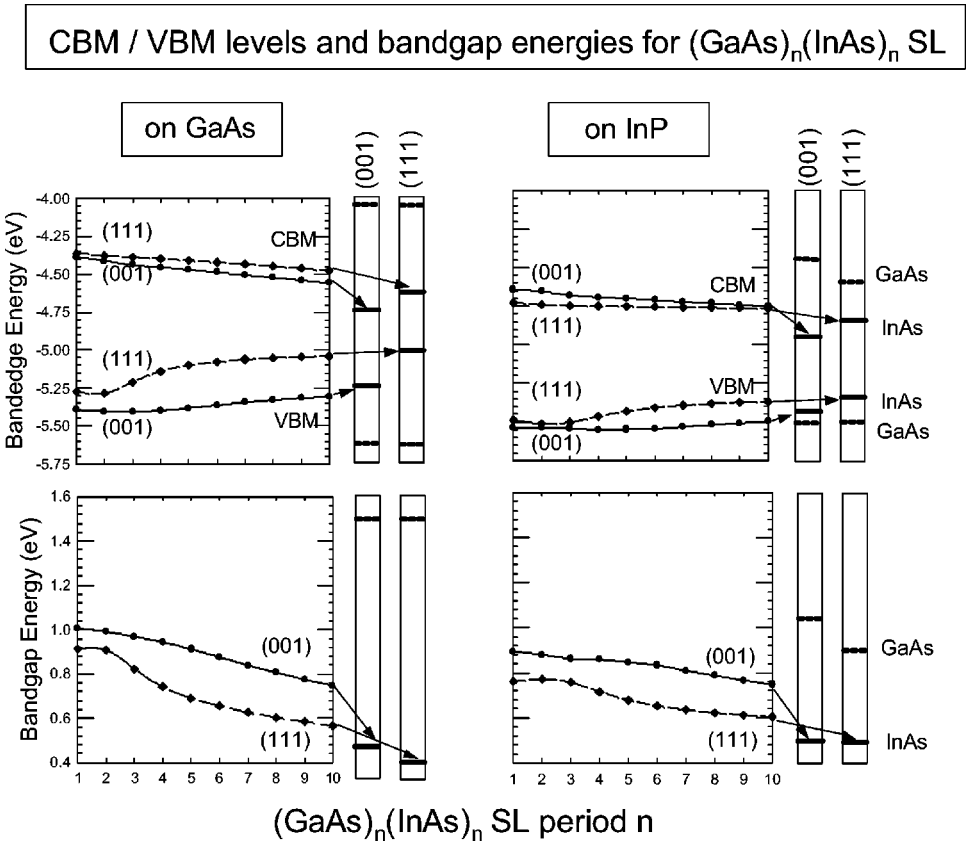

FIG. 7. The CBM and VBM levels for 001) and 111) $(GaAs)_n(InAs)_n$ superlattices on GaAs and InP. The boxes on the right-hand side of each panel depict the band edges of pure GaAs dashed lines) and pure InAs solid lines) binaries strained epitaxially on the corresponding substrate for the corresponding orientation. The two lower panels depict the band gaps.

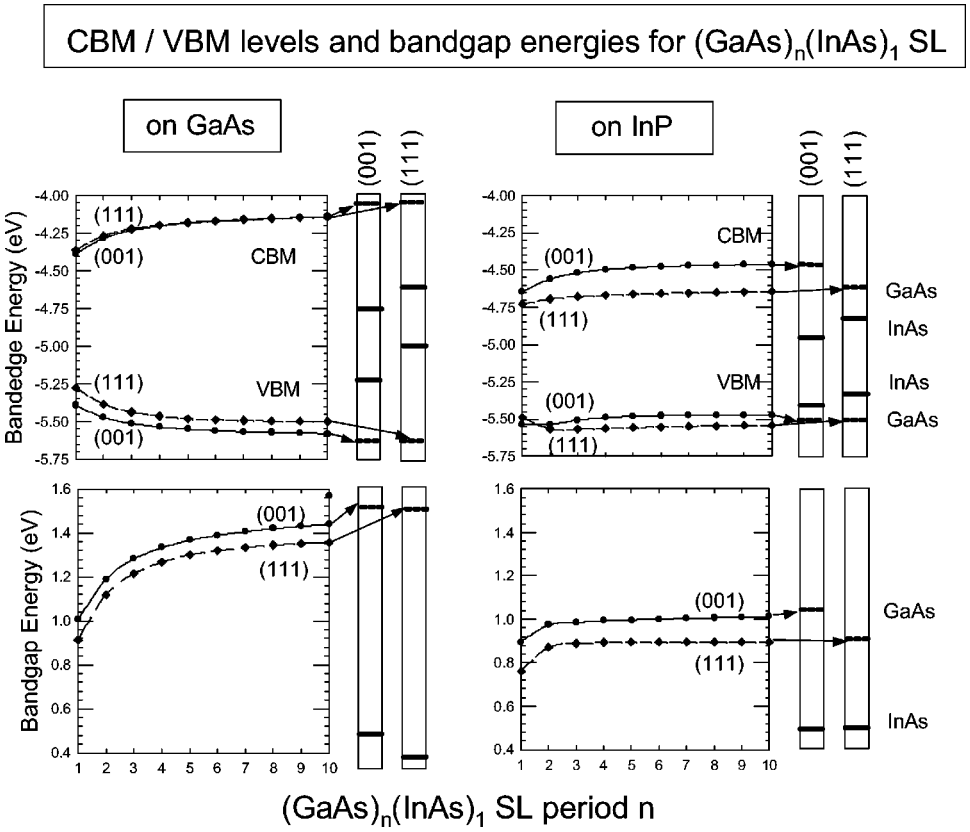

FIG. 8. The CBM and VBM levels and band gaps for 001) and 111) $(GaAs)_n(InAs)_1$ superlattices on GaAs and InP. The boxes on the right-hand side of each panel depict the band edges of pure GaAs and pure InAs binaries strained epitaxially on the corresponding substrate for the corresponding orientation.

of the 001) $(GaAs)_n(InAS)_n$ superlattice on InP for $n = 2$, 6, and 10. For the largest period shown, $n = 10$, the CBM states are localized on InAs, just as in the asymptotic behavior noted in Fig. 6. However, for shorter periods, Fig. 10 shows

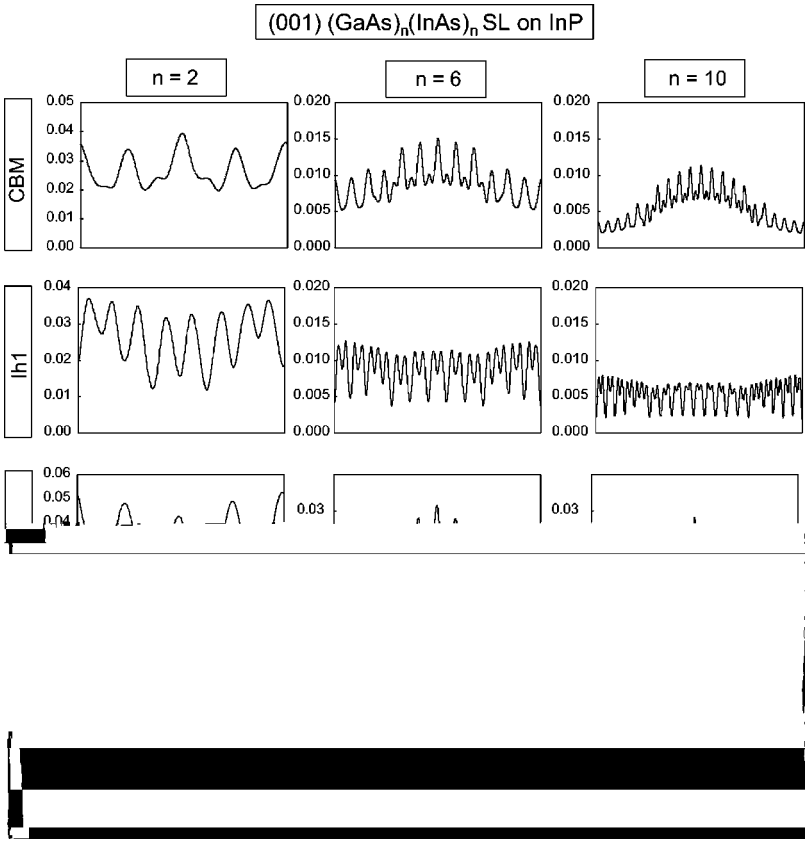

FIG. 10. The planar average of wave functions for 001) $(GaAs)_n(InAs)_n$ SL on InP for periods $n=2,6,10$ and for the states CBM, lh1, hh1, and hh2.

APPENDIX A: CALCULATION OF THE LOCAL STRAIN

To use the empirical pseudopotential, one needs a method to calculate the local strain for arbitrary systems. Figure 12 illustrates how the local strain is calculated. After the atomic positions are relaxed by minimizing the elastic energy, the local strain tensor ϵ_{ij} is calculated at each atomic site by considering the tetrahedron formed by the four nearest neighbor atoms. The distorted tetrahedron edges, $\mathbf{R}_{12}, \mathbf{R}_{23}$, and $\mathbf{R}_{34}$ are related to the ideal tetrahedron edges $\mathbf{R}_{12}^0, \mathbf{R}_{23}^0$, and $\mathbf{R}_{34}^0$ via which

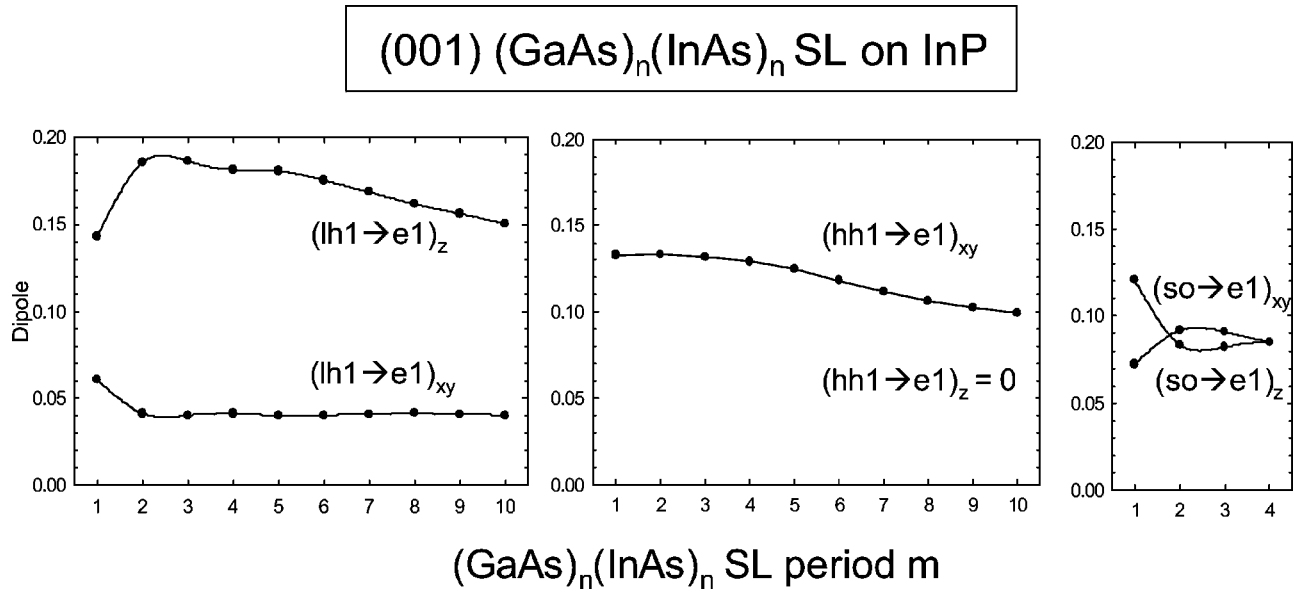

FIG. 11. The dipole elements for interband transitions in 001) $(GaAs)_n(InAs)_n$ SL on InP.

$$\begin{pmatrix} R_{12,x} & R_{23,x} & R_{34,x} \\ R_{12,y} & R_{23,y} & R_{34,y} \\ R_{12,z} & R_{23,z} & R_{34,z} \end{pmatrix} = \begin{pmatrix} 1+\epsilon_{xx} & \epsilon_{yx} & \epsilon_{zx} \\ 1+\epsilon_{xy} & 1+\epsilon_{yy} & \epsilon_{zy} \\ \epsilon_{xz} & \epsilon_{yz} & 1+\epsilon_{zz} \end{pmatrix} \times \begin{pmatrix} R^0_{12,x} & R^0_{23,x} & R^0_{34,x} \\ R^0_{12,y} & R^0_{23,y} & R^0_{34,y} \\ R^0_{12,z} & R^0_{23,z} & R^0_{34,z} \end{pmatrix}. \quad \text{A1)}$$

The ideal tetrahedron edges are $\{\mathbf{R}^0\}=\{[110]a/2,[0\bar{1}1]a/2,[\bar{1}10]a/2\}$, where a denotes the equilibrium lattice constant. The local strain, ϵ_{ij} is then calculated by a matrix inversion as

$$\begin{pmatrix} 1+\epsilon_{xx} & \epsilon_{yx} & \epsilon_{zx} \\ 1+\epsilon_{xy} & 1+\epsilon_{yy} & \epsilon_{zy} \\ \epsilon_{xz} & \epsilon_{yz} & 1+\epsilon_{zz} \end{pmatrix} = \begin{pmatrix} R_{12,x} & R_{23,x} & R_{34,x} \\ R_{12,y} & R_{23,y} & R_{34,y} \\ R_{12,z} & R_{23,z} & R_{34,z} \end{pmatrix} \begin{pmatrix} R^0_{12,x} & R^0_{23,x} & R^0_{34,x} \\ R^0_{12,y} & R^0_{23,y} & R^0_{34,y} \\ R^0_{12,z} & R^0_{23,z} & R^0_{34,z} \end{pmatrix}^{-1} - I, \quad \text{A2)}$$

where I is the unit matrix.

Since only the trace of the strain is required, the evaluation of Tr(ϵ) can be simplified as

$$\text{Tr}\ \epsilon) = \frac{\Delta V}{V} = \frac{\mathbf{R}_{12}\times\mathbf{R}_{13})\dot{\mathbf{R}}_{14}/6}{V} - 1, \quad \text{A3)}$$

where V is the volume of the ideal, undistorted tetrahedron, i.e., $V=(\mathbf{R}^0_{12}\times\mathbf{R}^0_{13})\dot{\mathbf{R}}^0_{14}/6$.

APPENDIX B: CALCULATION OF THE SPIN-ORBIT INTERACTION

The spin-orbit interaction is included in the Hamiltonian via a nonlocal, atom-centered p-like potential. In order to maintain linear scaling with system size, we use the ''small box'' implementation of Ref. 62 to evaluate the potential.

The spin-orbit term in the Hamiltonian, Eq. 16), consists of finite-ranged, atom-centered potentials, assumed zero for $r \geqslant r_{cut}$. Only the part of ψ within r_{cut} has contributions to $\hat{V}_{SO}\psi(\mathbf{r})$, which leads to the following implementation. For a given atom at $\mathbf{R}_i$, on the real-space numerical grid, we consider a small box centered on $\mathbf{R}_i$. Defining $\psi_Q(\mathbf{r}) \equiv \psi(\mathbf{r})$ for grid points inside the small box Q, we then treat ψ_Q as if it were periodic within the small box. This permits us to use the fast Fourier transform of $\psi_Q(\mathbf{r})$, $\psi_Q(\mathbf{G}_Q)$, where $\mathbf{G}_Q$ is a reciprocal lattice vector of the small box Q. Now in Fourier space, we can directly evaluate the nonlocal spin-orbit potential, $v_Q(\mathbf{G}_Q,\mathbf{G}'_Q)$,

$$_Q\ \mathbf{G}_Q) = \sum_{\mathbf{G}'} v_Q\ \mathbf{G}_Q,\mathbf{G}'_Q)\psi_Q\ \mathbf{G}'_Q). \quad \text{B1)}$$

Fourier transforming the new wave function $_Q$ back to real space we then add this small box of wave function back to the full wave function. The computational effort for each atom is therefore fixed, independent of the total size of the system, and the cost of the method scales linearly with the size of the system.

For the spin-orbit potential itself, we adopt a Gaussian form, $v_p(r)=\exp[-(r/0.7)^2]$, and rescale the amplitude of this potential for different atoms.

[1] P. Voisin, M. Voos, J.Y. Marzin, M.C. Tamargo, R.W. Nahory, and A. Cho, Appl. Phys. Lett. **48**, 1476 1986).

[2] M. Razeghi, P. Maurel, F. Omnes, and J. Nagel, Appl. Phys. Lett. **51**, 2216 1987).

[3] H. Ohno, R. Katsumi, T. Takamu, and H. Hasegawu, Jpn. J. Appl. Phys. **24**, L682 1985).

[4] T. Fukui and H. Saito, Jpn. J. Appl. Phys. **23**, L521 1984).

[5] M.A. Tischler, N.G. Anderson, and S.M. Bedair, Appl. Phys. Lett. **49**, 1199 1986).

[6] M.A. Tischler, N.G. Anderson, and S.M. Bedair, Appl. Phys. Lett. **50**, 1266 1987).

[7] J.M. Gereard and J.Y. Marzin, Appl. Phys. Lett. **53**, 568 1988).

[8] O. Brandt, K. Ploog, L. Tapfer, M. Hohenstein, R. Bierwolf, and F. Phillipp, Phys. Rev. B **45**, 8443 1992).

[9] J.C. Woicik, K.E. Miyano, J.G. Pellegrino, P. Shaw, S.H. Southworth, and B.A. Karlin, Appl. Phys. Lett. **68**, 3010 1996).

[10] J.C. Woicik, J.G. Pellegrino, S.H. Southworth, P.S. Shaw, B.A. Karlin, C.E. Bouldin, and K.E. Miyano, Phys. Rev. B **52**, 2281 1995).

[11] Y. Zheng, J.C. Bouillard, B. Capelle, A. Lifchitz, and S. Lagomarsino, Europhys. Lett. **41**, 623 1998).

[12] J. C. Woolley, in *Compound Semiconductors*, edited by R. K. Willardson and H. L. Goering Reinh5 1.9998 0.f 0.333 0 4d5rl 6.486H55rlY

Superlattices Microstruct. **3**, 539 1987).
[19] S.H. Pan, H. Shen, Z. Hany, F.H. Pollak, W. Zhuang, Q. Xu, A.P. Roth, R.A. Masut, C. Lacelle, and D. Morris, Phys. Rev. B **38**, 3375 1988).
[20] J.Y. Marzin and E.V.K. Rao, Appl. Phys. Lett. **43**, 560 1983).
[21] A. Zunger, MRS Bull. **23**, 35 1998).
[22] M. Grundmann, D. Biemberg, and N. N. Ledentson, *Quantum Dot Heterostructures* Wiley, New York, 1998).
[23] T. Lundstrom, W.V. Schoenfeld, H. Lee, and P.M. Petroff, Science **286**, 2312 1999).
[24] R.G. Dandrea and A. Zunger, Phys. Rev. B **43**, 8962 1991).
[25] D.L. Smith and C. Mailhiot, Rev. Mod. Phys. **62**, 173 1990).
[26] Y.C. Chang and J.N. Schulman, Appl. Phys. Lett. **43**, 536 1983).
[27] L.J. Sham and Y.T. Lu, J. Lumin. **44**, 207 1989).
[28] G. Edwards and J.C. Inkson, Solid State Commun. **89**, 595 1994).
[29] K.A. Mader and A. Zunger, Phys. Rev. B **50**, 17 393 1995).
[30] D.M. Wood and A. Zunger, Phys. Rev. B **53**, 7949 1996).
[31] L.W. Wang, S.H. Wei, T. Mattila, A. Zunger, I. Vurgaftman, and J.R. Meyer, Phys. Rev. B **60**, 5590 1999).
[32] R. Magri, L.W. Wang, A. Zunger, I. Vurgaftman, and J.R. Meyer, Phys. Rev. B **61**, 10 235 2000).
[33] D. Gershoni, C.H. Henry, and G.A. Baraff, IEEE J. Quantum Electron. **29**, 2433 1993).
[34] M.G. Burt, J. Phys. C **4**, 6651 1992).
[35] L.R. Ram-Mohan, K.H. Yoo, and R.L. Aggarwal, Phys. Rev. B **38**, 6151 1988).
[36] A. B. Chen and A. Sher, *Semiconductor Alloys* Plenum, New York, 1995).
[37] A. Zunger, S.-H. Wei, L.G. Ferreira, and J. Bernard, Phys. Rev. Lett. **65**, 353 1990).
[38] J.E. Bernard and A. Zunger, Phys. Rev. B **36**, 3199 1987).
[39] R. Magri, S. Froyen, and A. Zunger, Phys. Rev. B **44**, 7947 1991).
[40] S.-H. Wei and A. Zunger, Phys. Rev. B **43**, 1662 1991).
[41] S.-H. Wei and A. Zunger, Phys. Rev. Lett. **76**, 664 1996).
[42] P.R.C. Kent and A. Zunger, Phys. Rev. Lett. **86**, 2613 2001).
[43] *Electronic Density Functional Theory*, edited by J. F. Dobson, G. Vignale, and M. P. Das Plenum, New York, 1996).
[44] L. Hedin, J. Phys. C **11**, 489 1999).
[45] P. Hohenberg and W. Kohn, Phys. Rev. **136**